29 Jan 2021

REVISED REPLY TO COMMENT of *Yamamoto et al* on « Batsi et al, 2018, An Alternative View of the Microseismicity along the Western Main Marmara Fault, *Bull. Seism. Soc. Am.*, doi :10.1785/0120170258 »

By Evangelia Batsi[1], Anthony Lomax[2], Jean-Baptiste Tary[3], Frauke Klingelhoefer[1], Vincent Riboulot[1], Shane Murphy[1], Stephen Monna[4], Nurcan Meral Özel[5], Hakan Saritas[6], Günay Cifçi[6], Namik Çagatay[7], Luca Gasperini[8], Louis Géli[1]

1. Institut français de recherche pour l'exploitation de la mer (Ifremer), Marine Geosciences Research Unit, CS 70, 20280 Plouzané, France
2. ALomax Scientific, 320 Chemin des Indes, 06370, Mouans Sartoux, France
3. Universidad de los Andes, Departamento de Geociencias, Bogota DC, Columbia
4. Istituto Nazionale di Geofisica e Vulcanologia (INGV), Via di Vigna Murata, 605, 00143 Roma, Italy
5. Kandili Observatory and earthquake research institute (KOERI), 34684 Cengelkoy – Istanbul / TURKEY
6. Dokuz Eylül University (DEU), Cumhuriyet Bulvarı No: 144 35210 Alsancak / İZMİR, Turkey
7. Istanbul Technical University (ITU), Department of Geology, Faculty of Mines, 34469 Maslak, Istanbul, Turkey

In their comment, Yamomoto and co-authors are primarily concerned with the existence and effect of large values of minimum and maximum phase residuals in our analysis and locations using the 2014 observations, as listed in Tables S7 and S8 in the supplementary material of our paper (Batsi et al, 2018). We retain these large residuals in the tables and analysis since they have vanishingly small effect on the NonLinLoc locations, since the used, equal differential time (EDT) location algorithm (Lomax, 2008; Lomax et al., 2009) is highly robust to outlier readings. In the case of our Marmara study, phases with residuals larger than 1-2sec have near zero weight in the locations and corrected phase data. However, we agree the larger residuals may have had adverse effect on the generation of station corrections, though this, in turn, would also be mitigated by the robust location procedure. As a result, we consider that the location discrepancies between Yamomoto *et al* (2017) and Batsi et al. (2018) are not due to effects of excessively large residuals on the station corrections or locations. Instead, we propose that, as in many seismicity studies, error and uncertainty in the absolute hypocenter locations is primarily related to error in the velocity model and insufficient geometrical coverage of the source zones by the available seismic stations.

To support this proposition, and following the recommendation of Yamamoto et al., we recalculate station corrections for our 2014 data set and then relocate the 14 common events (Table A) that were located by both Yamamoto et al. (2017) and ourselves (see Table 9 in Batsi et al., 2018, with correct Yamomoto's location for event 3: 40.8058N, 27.9504E, 13.411km). We first generate station corrections as described in Batsi et al. (2018) using all events from 2014 which comply with the Batsi et al. (2018) location criteria (number of stations ≥ 5; number of phases ≥ 6; (3) root mean square (rms) location error ≤ 0.5s; azimuthal gap ≤ 180°), except that

we explicitly exclude from the analysis any P or S residuals > 3.0s when generating station corrections (Table B). We then relocate in the high-resolution, 3D, P-velocity model, as described in Batsi et al. (2018), the 14 common events using these station corrections. Figure 1 shows, for the 14 common events listed I Table A, the absolute NonLinLoc maximum likelihood and expectation hypocenters, and location probability density (pdf) clouds for our absolute relocations, along with the corresponding Yamamoto et al. (2017) double-difference relocations and Batsi et (2018) relative (NonDiffLoc) locations.

For sake of clarity, calculation results are detailed in Figure 2 for each individual event (1 to 14). The full information on the earthquake location spatial uncertainty is shown by the pdf clouds, while the maximum-likelihood hypocenter is the best solution point and the expectation hypocenter shows a weighted mean or "center of mass" of the cloud. The pdf clouds show a large uncertainty in hypocenter depth, the formal standard error in depth ranges from 2-9km. There is also a large separation between the maximum likelihood and expectation hypocenters for some events. These results underline the large uncertainty in depth determination and corresponding instability in any one-point measure chosen as a hypocenter. However, despite these uncertainties and instabilities, the Yamamoto et al. (2017) hypocenters remain generally deeper than the maximum likelihood and expectation hypocenters for our relocations, positioned towards the deeper uncertainty limits of our locations (e.g. the lower portion of the pdf clouds), and the Yamamoto et al. (2017) epicenters fall near the Main Marmara fault (MMF) while our relocated epicenters define off axis seismicity, along secondary faults from the MMF system. Thus our relocated events, which explicitly exclude excessively large residuals, still show differences with the Yamamoto et al. (2017) events, but not as large as those we found in our original study. Based on our recalculated NonLinLoc absolute locations, we suspect that Yamamoto et al (2017) results are systematically too deep and Batsi et al (2018) systematically too shallow, compared to what should be expected.

These differences in epicenter and depth, along with the size and shape of the pdf clouds for our relocations, are most easily explained by differences in the 3D velocity models and by differences in available stations and the consequent network geometry . However, while the epicentral distances at most of the OBS stations are shorter than the focal depths, as noted by Yamomoto et al., the elongation of our pdf clouds in depth suggests that an increase in network aperture with more distant stations, along with an accurate 3D model, is required to better constrain depth.

High-resolution earthquake epicenter and depth determinations below the Sea of Marmara is a difficult problem, yet of critical importance. To better understand why the two studies produce different results, and to obtain the best possible locations, the best action is to increase the number of constraints by merging the two OBS datasets, and examine, step by step, the effects of locations methods, network geometry and 3D velocity models from the two studies. Sharing the data (or phase picks and model) would provide an unique opportunity to give real, direct insight into these issues. We suspect that epicenters will shift as a function of used velocity model and station set, and that in all cases depth uncertainty is large, as is clearly represented in the NonLinLoc location, pdf clouds, while linearized location error estimates usually show lower uncertainty.

References:

Batsi E., Lomax A., Tary J-B. et al. (2018). An alternative view of the micro-seismicity along the western main Marmara fault, *Bull. Seismo. Soc. Am.*, **108** (5A), doi:10.1785/0120170258.

Lomax, A., Anthony Lomax Scientific Software website, http://alomax.free.fr

Lomax A. 2008. Location and tectonics of the focal region of the California earthquake of 18 April 1906, Bull. Seismol. Soc. Am. 98, 846–860.

Lomax A., Michelini A., and Curtis A. 2009. Earthquake location, direct, global-search methods, in complexity, in Encyclopedia of Complexity and System Science, Part 5, Springer, New York, New York, 2449–2473, doi: https://doi.org/10.1007/978-0-387-30440-3

Yamamoto, Y., Takahashi N., Pinar A., Kalafat D., Citak S., Comoglu M., Polat R., and Kaneda Y. (2017). Geometry and segmentation of the North Anatolian fault beneath the Marmara Sea, Turkey, deduced from long-term ocean bottom seismographic observations, *J. Geophys. Res. Solid Earth*, **122**, doi:10.1002/2016JB013608

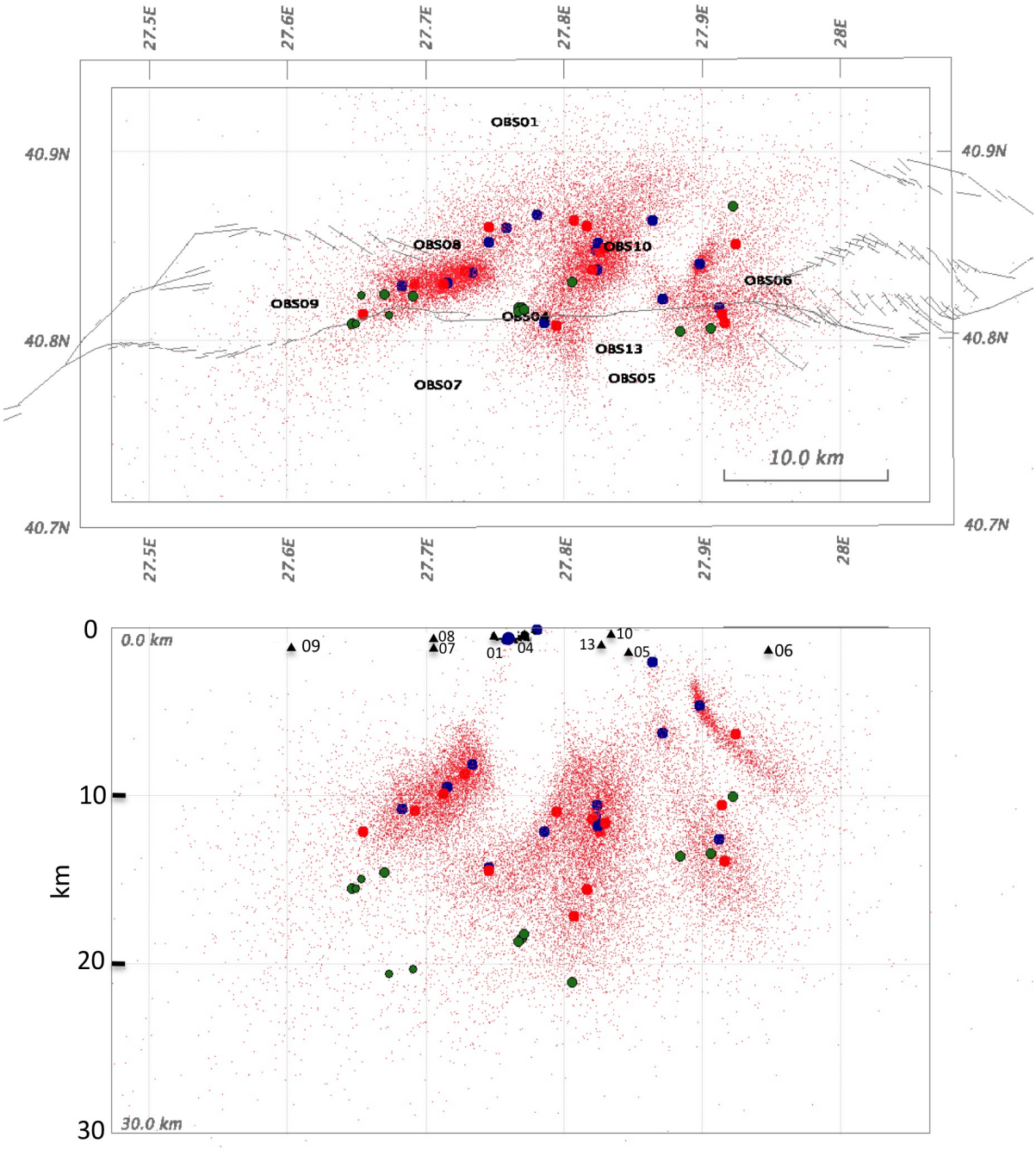

Figure 1. Map view (upper) and section view from South (lower) of locations for 14 common events (Table 9 in Batsi et al, 2018, with Yamamoto et al (2017) location of event 3 now positionned at 40.8058N, 27.9504E, 13.411km). Our recalculated absolute locations are shown as location pdf clouds (red points), and maximum likelihood (solid blue circles) and expectation (solid red circles) hypocenters. Yamamoto et al (2017) double-difference relocations are shown as solid green circles. Gray lines indicate the main structural features of the Main Marmara fault. Black triangles are for OBS sites (deployment of 2014).

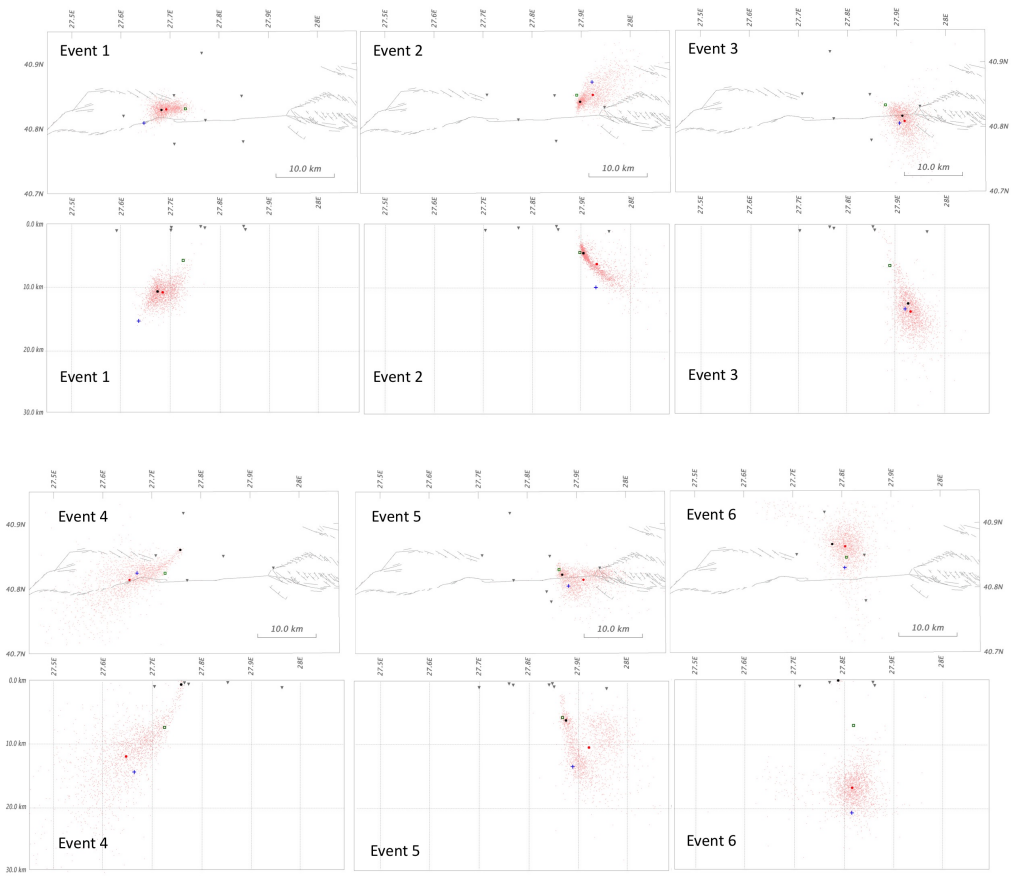

Figure 2a *: Details for each individual event (from 1 to 6) listed in Table B. Our recalculated, absolute NonLinLoc locations are shown as location pdf clouds (red points), and maximum likelihood (solid blue circles) and expectation (solid red circles) hypocenters. Yamamoto et al (2017) double-difference relocations are shown as blue crosses. Batsi et al (2018) relocations are shown as green squares. Note: the main issues are station corrections, available stations and model differences, all of these are issues of absolute event location. The relative locations will either be constrained to or will have a very strong tendency to preserve the absolute location centroid of highly correlated event clusters.*

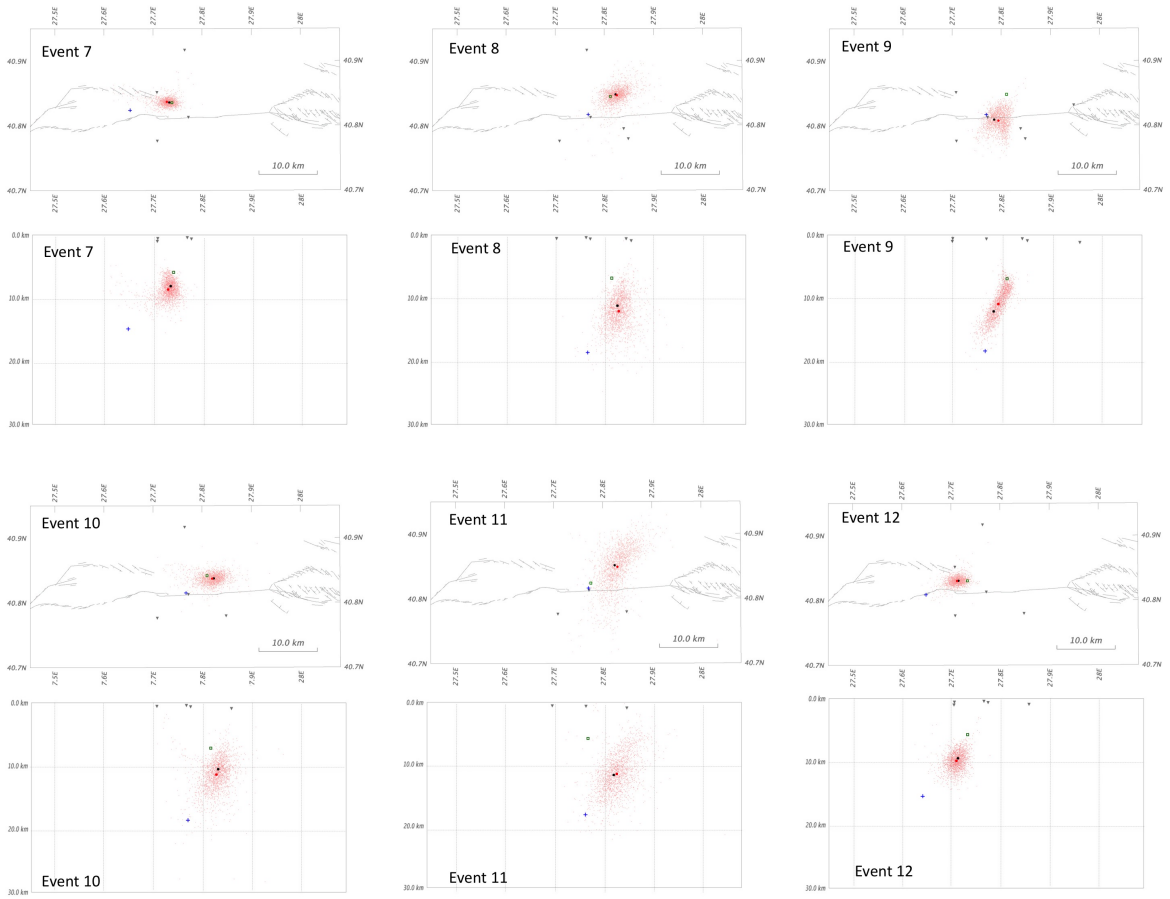

Figure 2b : Details for each individual event (from 7 to 12) listed in Table B. See caption in figure 2a.

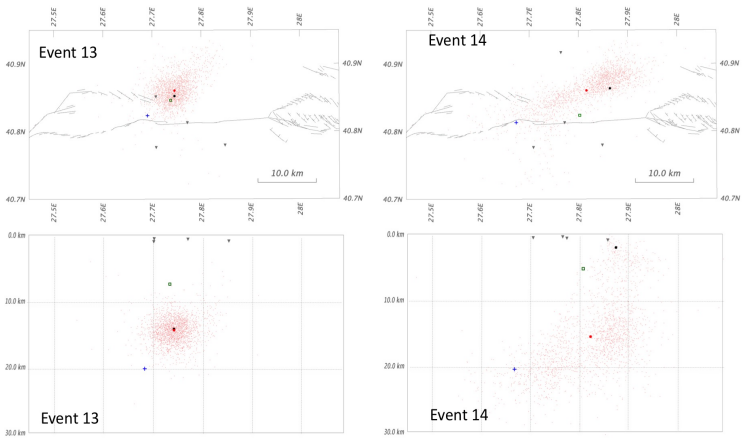

Figure 2c : Details for each individual event (from 13 to 14) listed in Table B. See caption in figure 2a.

		NonLinLoc											
		MAXIMUM LIKEHOOD			EXPECTATION			YAMAMOTO's et al (2017)			BATSI et al (2018)		
N°	Date (YEAR 2019) mo/dd hh:mn:ss	LAT	LON	Z bsl (km)	LAT	LON	Z bsl (km)	LAT	LON	Z bsl (km)	LAT	LON	Z bsl (km)
1	09/26 06:02:54.30	40.83	27.68	10.8	40.83	27.69	10.9	40.81	27.65	15.5	40.83	27.73	5.8
2	10/01 14:44:49.43	40.84	27.90	4.6	40.85	27.92	6.3	40.87	27.92	10.0	40.85	27.89	4.5
3	10/03 21:40:21.74	40.82	27.91	12.6	40.81	27.92	13.9	40.81	27.95	13.4	40.83	27.88	6.5
4	10/04 11:58:34.45	40.86	27.76	0.7	40.81	27.66	12.1	40.82	27.67	14.5	40.82	27.73	7.5
5	10/17 19:52:52.82	40.82	27.87	6.2	40.81	27.91	10.5	40.80	27.88	13.5	40.83	27.86	5.8
6	10/18 10:17:42.37	40.87	27.78	0.1	40.86	27.81	17.1	40.83	27.81	21.1	40.85	27.81	7.2
7	10/24 14:18:24.57	40.84	27.73	8.1	40.84	27.73	8.6	40.82	27.65	14.9	40.84	27.74	5.9
8	10/25 01:46:52.04	40.85	27.82	11.2	40.85	27.83	12.1	40.82	27.77	18.6	40.85	27.81	6.8
9	10/25 03:05:00.56	40.81	27.79	12.1	40.81	27.79	10.9	40.82	27.77	18.4	40.85	27.81	6.9
10	10/25 04:21:38.54	40.84	27.82	10.5	40.84	27.82	11.4	40.82	27.77	18.6	40.84	27.81	7.2
11	10/25 09:28:56:47	40.85	27.82	11.8	40.85	27.83	11.6	40.82	27.77	18.2	40.82	27.78	5.9
12	10/26 03:21:34:01	40.83	27.72	9.5	40.83	27.71	9.9	40.81	27.65	15.5	40.83	27.73	5.7
13	10/26 07:41:50.93	40.85	27.75	14.3	40.86	27.75	14.4	40.82	27.69	20.3	40.85	27.74	7.4
14	10/27 21:22:08:44	40.86	27.86	2.0	40.86	27.82	15.6	40.81	27.67	20.5	40.82	27.80	5.3

TABLE A: *Recalculated absolute NonLinLoc locations for the 14 common events listed in Table 9 of Batsi et al, 2018, with Yamamoto et al (2017) location of event 3 now positionned at 40.8058N, 27.9504E, 13.411km and with depths from Batsi et al (2018) here expressed in kilometers below sea-level. The maximum likelihood is the point with maximum pdf amplitude in the cloud, the expectation is the mean or barycenter (in xyz) of the points in the cloud weighted by their relative likelihood value*

Station	Phase	Nres	TotCorr (s)	StdDev (s)
OBS01	P	40	-0.082	0.302
OBS01	S	35	-0.047	0.532
OBS03	P	34	-0.435	0.552
OBS03	S	30	0.027	0.759
OBS04	P	47	-0.371	0.456
OBS04	S	39	0.262	0.617
OBS05	P	31	0.025	0.451
OBS05	S	34	0.184	0.724
OBS06	P	21	-0.080	0.623
OBS06	S	22	0.996	0.642
OBS07	P	38	-0.472	0.610
OBS07	S	37	0.517	0.659
OBS08	P	52	-0.022	0.221
OBS08	S	42	0.680	0.206
OBS09	P	5	-0.053	0.574
OBS09	S	4	3.371	1.262
OBS10	P	36	-0.042	0.162
OBS10	S	20	0.557	0.609
OBS11	P	6	-0.099	0.160
OBS11	S	16	0.253	0.542
OBS12	P	7	-0.221	0.374
OBS12	S	14	0.340	0.307
OBS13	P	12	0.361	0.534
OBS13	S	9	0.677	0.333

Table B: Total Phase Corrections (CalcResidual + InputDelay) recalculated at each OBS station. See details in main text.